Non-toxic and rapid chemical bath deposition for SnO_2 electron transporting layers in perovskite solar cells

Matthias J. Grotevent,[1,‡] Linda Kothe,[1,2,‡] Yongli Lu,[1] Chantalle Krajewska,[1] Meng-Chen Shih,[1] Shaun Tan,[1] Michael Tiemann[2], Moungi G. Bawendi[1*]

[1]Department of Chemistry, Massachusetts Institute of Technology, 77 Massachusetts Avenue, Cambridge, Massachusetts 02139, USA

[2]Paderborn University, Faculty of Science, Department of Chemistry, Warburger Str. 100, D-33098 Paderborn, Germany

E-mail: mgb@mit.edu

[‡]Both authors contributed equally to this work

[*]corresponding author

KEYWORDS: perovskite solar cell, chemical bath deposition, tin oxide, amorphous, metal oxide

Abstract. Perovskite solar cells are a promising new solar technology with efficiencies surpassing polycrystalline silicon solar cell technology. For the n-i-p perovskite solar cells, tin oxide is typically used as the electron transport layer. One typical deposition method is chemical bath deposition. However, the drawbacks are toxic precursors and the slow reaction driven by dissolved oxygen forming SnO_{2-x}. Here, we present a tin oxide chemical bath deposition starting from non-toxic sodium stannate solutions. Within 6 minutes of reaction time, a 9 nm thick amorphous

Sn(IV)-oxide film is grown yielding solar cells with power conversion efficiencies of at least 23.2%. Surprisingly, the sole use of Sn(IV) precursors contradicts the previous Sn(II) doping assumption required for *n*-doping & high electric conductivity, and, unexpectedly, amorphous tin oxide films are as suitable for charge transport layers as their crystalline counterparts. The synthesis method is transferrable to other substrates (ITO, glass) and other thin-film metal oxide coatings (MoO_x, SiO_2) and beneficial for devices such as solar cells, photodetectors, light emitting diodes, and heterogeneous catalysis.

Introduction

Perovskite solar cells are one of the most promising emerging solar technologies, with power conversion efficiencies surpassing 26%.[1] The photoactive perovskite layer is sandwiched between an electron- and hole-transport layer. Tin(IV) oxide (SnO_2) as the electron transport layer (ETL) has attracted an increased interest due to its high photostability, ideal energy band alignment, efficient hole blocking & electron conducting property, low defect density, and low-temperature processability in comparison to TiO_2.[2] SnO_2 can be deposited using evaporation or from solution, for example, by thermal evaporation, sputtering, sol-gel, atomic layer deposition, or chemical bath deposition. The deposition methods are well summarized in a review article and citations therein.[3] Chemical bath deposition is particularly interesting due to its ability to produce uniform, compact, and pinhole-free thin films. In a typical reaction, a water-based Sn(II)-chloride solution combined with hydrochloric acid, thioglycolic acid, and urea reacts over about 12 hours, forming a nonstoichiometric SnO_{2-x} layer.[2,4–6] Recent adaptions of this synthesis replaced thioglycolic acid with oxalic acid.[7] This removes sulfur-containing precursors, potentially leading to contaminations and reduced device stability. Further, it lowers the reaction time down to 3

hours.[7] Others have replaced the Sn(II)-chloride and hydrochloric acid with Sn(II)-sulfate precursors, enabling the chemical bath deposition on chemically sensitive substrates such as indium-tin-oxide (which is chemically etched under hydrochloric acid conditions). However, the reaction times are still multiple hours.[8] In all of the aforementioned chemical bath depositions, urea decomposes and increases the pH value. At the same time, Sn(II) is oxidized to Sn(IV) from dissolved molecular oxygen. Therefore, two reactions are simultaneously changing the reaction conditions and products. The changes in the reaction conditions at an increased pH value result in a slightly nonstoichiometric SnO_{2-x}.[2,9] This continuous oxidation state change is believed to be desired for gradual doping within the SnO_2 layer, enabling excellent charge transfer.[2] However, dissolved oxygen, critical for the oxidation of Sn(II) to Sn(IV), must be present and is usually not accounted for. Quantifying the dissolved oxygen is cumbersome and dynamic due to the exposure of the reaction to the ambient atmosphere and subsequent oxygen diffusion from the atmosphere into the solution. Notably, industrial applications require a fast and highly reproducible layer deposition with synthesis times below 15 minutes—a highly challenging task. Additional steps, such as post-synthesis annealing at 170 °C for 60 minutes in air, are typically performed, but long annealing times are also problematic for commercial processing. The annealing step is usually required to reduce the surface defect density and remove unwanted organic contaminations originating from precursors.[2,7]

Besides the direct growth of SnO_2 on substrates by chemical bath deposition, SnO_2 nanoparticles can be synthesized, for example, from tin(II) halides such as $SnCl_2$,[10,11] SnF_2,[12] and $SnCl_4$.[13] Furthermore; a few reports grow SnO_2 from tin(IV) stannates, e.g., the growth of SnO_2 shells on Au nanoparticles by thermal decomposition of the stannate at 60 °C over one hour,[14] or the synthesis of spherical SnO_2 nanoparticles of about 30 nm size by thermal decomposition of

sodium stannate over 5 hours at 150 °C (pressurized water).[15] While those reactions take hours, their final deposition from solution can be faster, for example, by slot-die coating and blade coating; however, thicker coatings are required for nanoparticle films to ensure a pinhole-free and conformal layer.

Here, we present a rapid (within 6 minutes), simple chemical bath deposition of SnO_2 from non-toxic Sn (IV) stannate in water without any additional chemicals. The reaction is simply based on the thermal decomposition of the stannate. Solar cell power conversion efficiencies of at least 23.2% are demonstrated on par with the fabricated reference devices. In addition to the fabrication on fluorine-doped tin-oxide substrates, the mild reaction conditions enable the chemical bath deposition of SnO_2 on chemically sensitive substrates such as indium tin oxide. In addition, post-synthesis thermal annealing is not required, further simplifying device fabrication. This method is not limited to the deposition of tin oxide; it can also be applied to other water-soluble oxometallates to form thin films, such as molybdenum (VI) oxide and silicon dioxide.

Results and Discussion

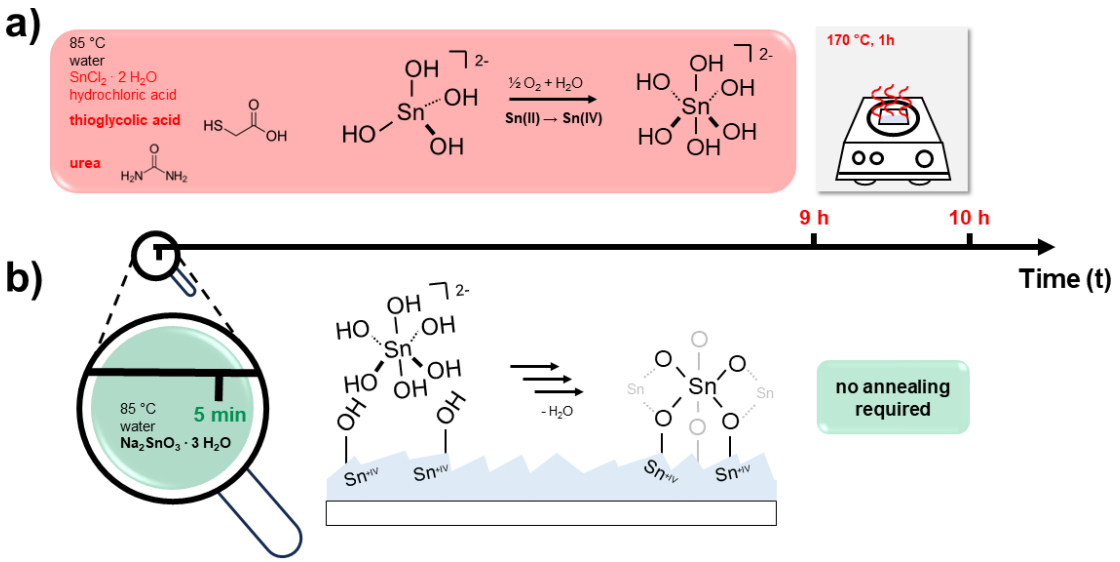

Figure 1. Schematic comparison *of the SnO_2 chemical bath deposition from a) Sn(II) chloride and b) sodium stannate.*

Figure 1a displays the reaction components for a typical chemical bath deposition. The reaction is based on a complex mechanism with various side reactions and uncontrolled Sn(II) oxidation to Sn(IV) over a few hours. A novel and simple chemical bath deposition (Figure 1b) is investigated using low-cost water-soluble stannate precursors such as sodium stannate ($Na_2SnO_3 \cdot 3H_2O$). The precursor is readily solubilized in deionized water, resulting in a clear colorless solution followed by a condensation reaction of the in-situ formed hexahydroxostannate complexes, resulting in a fast and controllable thin-film deposition. While hexahydroxostannate solutions are meta-stable for weeks at room temperature, the solution slowly becomes hazy, indicating a destabilization and condensation reaction towards SnO_2. The chemical reaction can be described with the following equation:

$$Na_2SnO_3 \cdot 3\,H_2O \equiv Na_2[Sn(OH)_6] \rightarrow SnO_2 \downarrow + 2\,NaOH + 2\,H_2O$$

The equation indicates a pH change; sodium stannate solutions (typically 0.1M) are already basic with a pH of 12 at room temperature, and a slight increase in the pH value towards 12.4 was observed after the chemical bath deposition reaction. SnO_2 has been reported to be chemically stable below a pH of 11.5,[15] we observed nucleation and growth even at a pH of 12.4. The homogeneous nucleation from sodium stannate in solution is based on the condensation from two octahedral coordinated stannate complexes $[Sn(OH)_6]^{2-}$.[15] Surface hydroxy-groups from FTO (fluorine-doped tin (IV) oxide) substrates may well serve as nucleation centers facilitating a competing templated heterogeneous film growth. Due to the simplicity of the reaction, the reaction parameters can be limited to the reaction temperature, stannate concentration, and growth time. Those parameters were investigated in Figure 2, starting with the reaction temperature between

55 °C and 85 °C (Figure 2a, SEM images in Supplementary Figure 1a). The reaction time was adjusted to a point where homogeneous particle formation was visibly observed, ranging from 45 minutes at lower temperatures to 6 minutes at 85 °C. A decrease in solar cell efficiency is observed when substrates are grown at higher temperatures; however, this may originate from non-optimized reaction times as the device efficiency is highly dependent on the layer thickness. The homogeneous particle growths determined the reaction time, which does not necessarily reflect the optimal heterogeneous growth times. As the reaction works at all of the tested temperatures, higher temperatures are chosen with the advantage of faster film growth. Therefore, the reaction as a function of the stannate concentration was further investigated at a temperature of 85 °C (Figure 2b, SEM in SI Figure 1b). The reaction was quenched at the point of visible homogeneous particle formation from 20 minutes at lower to 5.5 minutes at high precursor concentrations. The reactions were stopped once visible particle formation was observed in the solution. This can be improved by optimizing the reaction time at a fixed bath temperature of 85 °C and precursor concentration of 0.1 M (Figure 2c). This time, the reaction is not stopped by the appearance of homogeneous particle formation but by the reaction time, resulting in a higher reproducibility. The solar cell efficiency increases up to a reaction time of 6 minutes, and the observed hysteresis narrows down simultaneously. If desired, the reaction can be further accelerated at higher reaction temperatures and precursor concentrations, leading to shorter reaction times. Scanning electron microscopy images of the coated and one uncoated FTO substrate (as reference) are shown in Figure 2d. The film growth can be described following two distinct film growth mechanisms discussed in the literature: an ion-by-ion growth directly on the substrate and a homogeneous nanoparticle growth with subsequent nanocrystal attachment to the substrate.[3,7,9,13] A combination of both growth mechanisms would also be plausible, and individual growth mechanisms may be specific to any

underlying growth conditions (e.g., the presence of additives in solution).[9] The scanning electron microscopy images in Figure 2d strongly indicate an ion-by-ion growth: the films were grown in the same growth solution and taken out one after another at different reaction times; simultaneously, nanoparticles formed within the solution. Therefore, a nanoparticle formation in solution and subsequent attachment to the film should lead to drastic changes in the film smoothness of two subsequent films. The smoothness of the films for all growth times strongly indicates an ion-by-ion growth mechanism, while some attached nanoparticles can be observed for one sample. Those particles may have been attached by chance to the film during the removal of the substrate from the growth solution. While this study optimized the chemical bath deposition of SnO_2 from sodium stannate, other water-soluble stannate sources, such as potassium stannate, can also be used (Supplementary Figure 2). Furthermore, the reaction is not limited to stannates; other water-soluble oxometallates, such as sodium molybdate and sodium metasilicate, can be used as precursors forming coatings of molybdenum(VI) oxide and silicon(IV) oxide, respectively (Supplementary Figure 3).

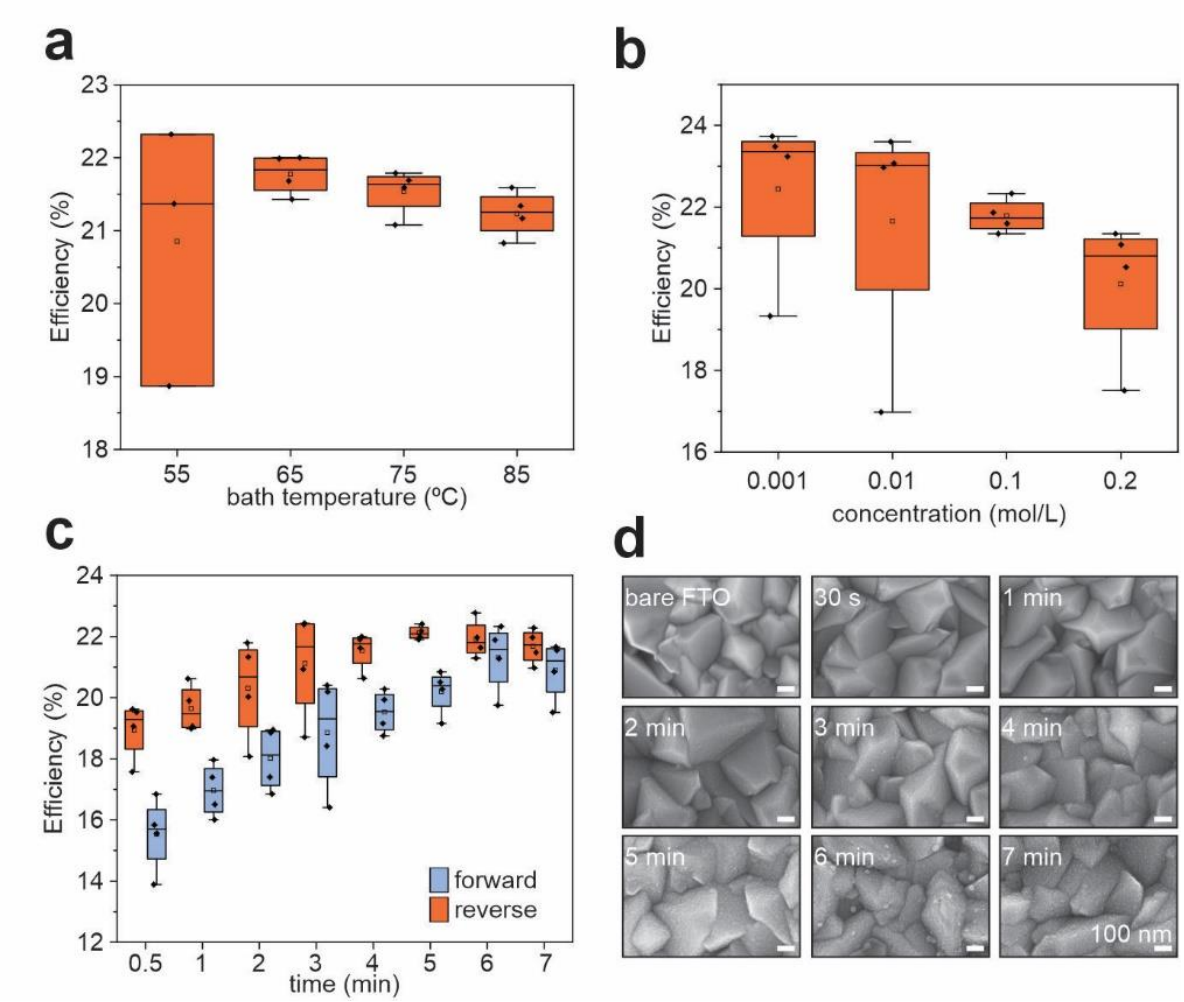

Figure 2. SnO_2 chemical bath deposition under various reaction conditions. *Solar cell efficiency as a function of a) reaction bath temperature (0.1M stannate concentration), b) $Na_2SnO_3 \cdot 3H_2O$ concentration (bath temp.: 85 °C), c) reaction time (bath temp.: 85 °C, 0.1M concentration), and d) scanning electron microscopy images of the SnO_2/FTO substrates at respective growth times.*

Figure 3 compares the chemical bath depositions from $SnCl_2$ with the reaction from sodium stannate solutions. Scanning electron microscopy images (Figure 3a, b) reveal that both reactions produce densely compact films with continuous coverage. The morphology exhibits a rougher surface for films grown with Sn(II)-chloride potentially originating from the additives (functioning as ligands) such as urea and thioglycolic acid (or oxalic acid). This surface roughness could negatively affect conductivity and device performance;[16] however, the solar cell efficiencies from

the respective films (Figure 3c) lead to the exact same device efficiencies. This surprises, as the established synthesis route from Sn(II) precursors is believed to require the formation of impurity doping (SnO_{2-x}), resulting in a *n*-type semiconductor for improved electrical conductivity. In comparison, the water-based stannate synthesis route starts from Sn(IV), and any significant Sn(II) doping seems unlikely due to the lack of reduction agents and the presence of dissolved molecular oxygen (oxidizing agent) in the solution. This is further supported by the fact that stoichiometric SnO_2 is a white powder, and SnO_{2-x} appears as a yellow powder.[10,11,15,17] The white color of the nanoparticles formed in solution from the stannate reaction indicates the absence of any significant Sn(II) doping. Therefore, the role of Sn(II) in the bulk of SnO_2 thin films remains a topic of discussion. The nonstoichiometric SnO_{2-x} surface, however, is unfavorable and presents additional charge trap states that potentially facilitate degradation of the adjacent perovskite layer.[7] Therefore, the Sn(II) chloride route requires a post-synthesis oxidation step by annealing the substrates for one hour at 170 °C, converting surface Sn(II) to Sn(IV).[7] This prolongs the overall fabrication by another hour, which is unsuitable for scale-up and industrial use. On the contrary, the sodium stannate synthesis route leads to surface Sn(IV) and does not require any post-synthesis annealing step: no efficiency difference has been observed between annealed and non-annealed substrates (Figure 3d). This highlights the advantages of the sodium stannate chemical bath deposition by starting from Sn(IV): (I) fast SnO_2 film growth within minutes (no oxidation step required), (II) surface oxidation by annealing is not required, (III) no toxic chemicals and additives are used.

The direct, in-depth analysis of the thin SnO_2 on fluorine-doped SnO_2 (FTO) substrates is highly challenging due to the low spatial dimensionality of the SnO_2 film and the similarity of the film and growth substrate. A cross-sectional high-angle annular dark-field scanning transmission electron microscopy image (Figure 3e) shows a 9 nm thick amorphous SnO_2 layer grown on top

of an FTO substrate. The amorphous character is further supported with powder x-ray diffraction measurements from solution-grown SnO_2 nanoparticles (scanning electron microscopy image, Supplementary Figure 4), which do not show any significant diffraction peaks, indicating the growth of a primarily amorphous SnO_2 film (Supplementary Figure 5). In addition, a fast growth rate at low temperatures is usually associated with forming amorphous materials. In contrast, crystalline materials typically require slow growth and high temperatures to incorporate atoms perfectly into an organized crystal lattice. Electron energy loss spectroscopy (Figure 3f) was used further to analyze the oxidation state of the tin oxide layer. Typically, the tin oxidation state is indirectly investigated by looking at the energy-loss near-edge structure of the oxygen K-edge with an energy splitting of about 3.5 eV for Sn(II)-oxide and about 6 eV for Sn(IV)-oxide.[7,18] While the energy splitting is rather 6 eV (indicating Sn(IV) oxide), the height ratio of the two oxygen peaks is smaller and closer to the reference of the Sn(II) oxide spectrum. However, the literature reference spectra analyzed crystalline samples, and the amorphous character of our tin oxide layer may result in deviations from the literature spectra due to differences in the local chemical environment. Amorphous SnO_2 is likely nonstoichiometric, with hydroxy-groups incorporated into the film to fully coordinate the oxophilic Sn(IV). While trace amounts of Sn(II) cannot entirely be ruled out—even though unlikely due to the oxidative reaction conditions—it is surprising that amorphous Sn(IV)-oxide electron transport layers perform as well as representative crystalline films.

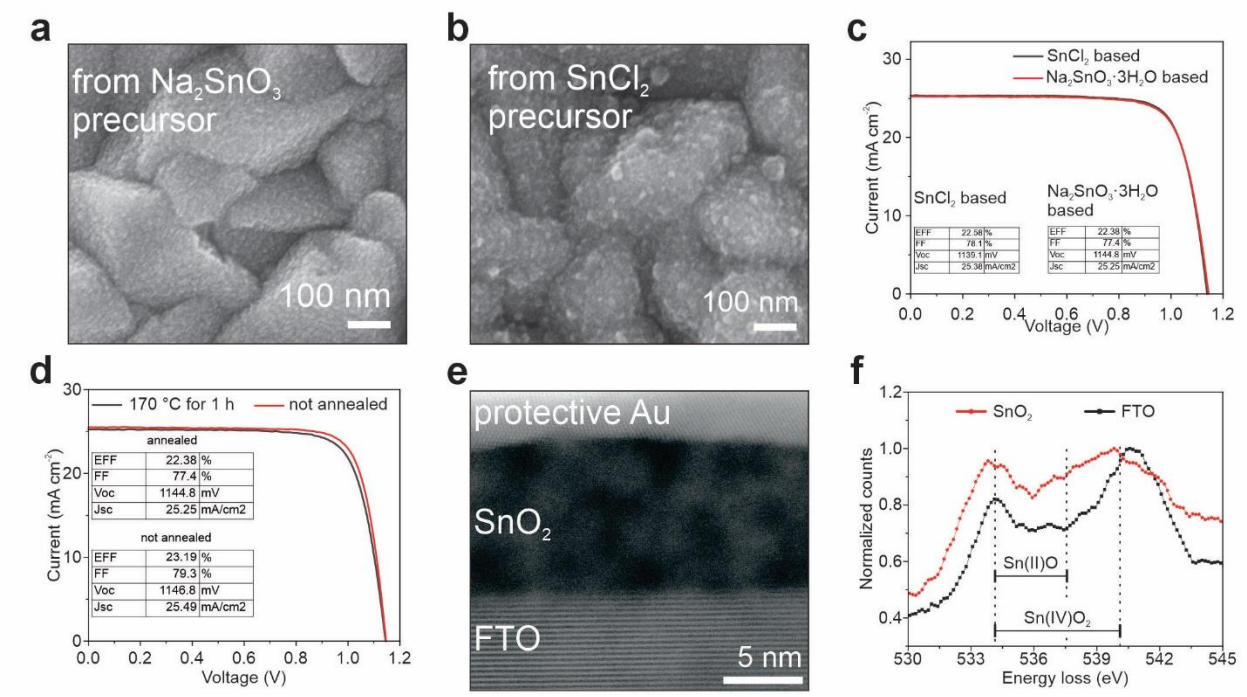

Figure 3. Analysis of SnO_2 grown from chemical bath deposition. *Scanning electron microscopy images from a) $Na_2SnO_3{\cdot}3H_2O$ precursor, b) from $SnCl_2$ precursor, c) solar cell device efficiency fabricated from SnO_2 grown with $SnCl_2$ or $Na_2SnO_3{\cdot}3H_2O$ precursors, d) solar cell device efficiency of a thermally annealed and non-annealed SnO_2 film, e) high-angle annular dark-field scanning transmission electron microscopy image of SnO_2 grown from stannate solutions on FTO, and f) electron energy loss spectroscopy of the respective films in (e).*

The basic reaction conditions of the chemical bath deposition from sodium stannate enable SnO_2 coatings on indium-tin-oxide (ITO) substrates, which would otherwise be chemically etched under prevalent acidic reaction conditions. The electron microscopy images in Figure 4a show pristine ITO and ITO coated with a continuous and homogeneous SnO_2 coating. Like the growth on FTO substrates, an ion-by-ion growth is initially observed within the first 10 minutes of growth. A higher degree of surface-attached nanoparticles can be observed for longer growth times. Compared to the coating on FTO, ITO substrates require a longer reaction time, with perovskite solar cell devices achieving a power conversion efficiency of at least 20% (Figure 4b, c). Like the SnO_2 coatings on FTO, the hysteresis is reduced at longer SnO_2 growth times. The demonstrated chemical bath deposition from sodium stannate is not restricted to FTO and ITO substrates; other

hydroxy-terminated substrates, such as glass, can also be coated. The demonstrated scalable SnO_2 thin film deposition method may be used, e.g., for solar cells, photodetectors, light emitting devices, and heterogeneous catalysis.

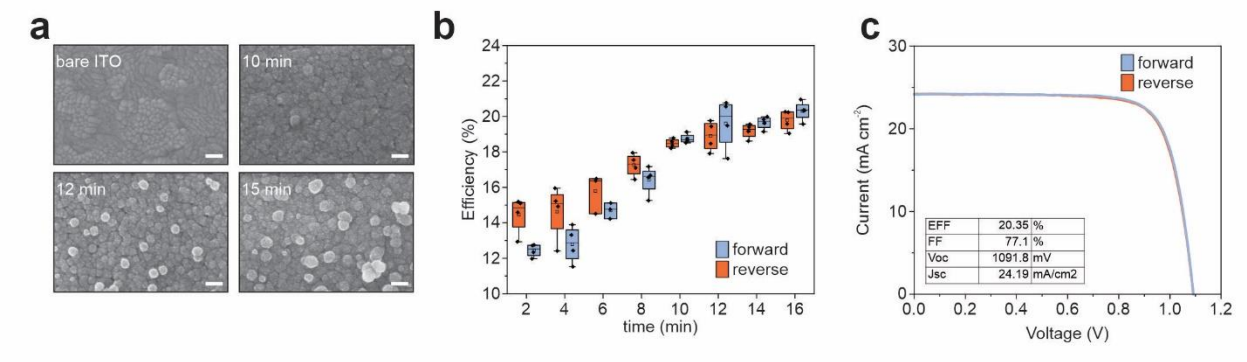

Figure 4. SnO_2 CBD from $Na_2SnO_3 \cdot 3H_2O$ precursor on ITO substrates. *a) scanning electron microscopy images at various growth times, b) solar cell efficiency as a function of growth time, and c) current-voltage measurement. Scale bars 100 nm.*

Conclusion

A tin oxide chemical bath deposition starting from Sn(IV) stannate instead of the typical Sn(II)-chloride synthesis route is presented. The Sn(IV) stannate synthesis cuts the reaction time from hours to 6 minutes, does not require any post-synthesis annealing step, uses only non-toxic precursors, and enables the synthesis on chemically labile substrates such as indium-tin-oxide. The device efficiency of perovskite solar cells fabricated from those substrates is on par with reference solar cells with at least a 23.2% power conversion efficiency. The fast synthesis produces a mostly amorphous film of about 9 nm thickness. Previous understandings of tin oxide-based electron transport layers required a Sn(IV) surface for a low density of charge carrier trap states but sufficient *n*-doping of SnO_2 by Sn(II) for improved electrical conductivity in the bulk. The presented results contradict the current opinion as solely Sn(IV) precursors have been used in water under oxidative reaction conditions—preventing the formation of Sn(II). It also highlights that

charge transport layers of amorphous metal oxide films can be as good as their crystalline counterparts. Overall, the presented progress enables the chemical bath deposition of tin oxide to be used for commercial application. Besides tin oxide, the presented method is transferable to other metal-oxide thin films, such as molybdenum(VI) oxide and silicon(IV) oxide, grown from water-soluble oxometallates.

Experimental Section

Chemicals: Sodium stannate trihydrate (95%, Sigma Aldrich), potassium stannate trihydrate (99.9% trace metal basis, Sigma Aldrich), sodium molybdate dihydrate (≥99%, Sigma Aldrich), sodium metasilicate (Sigma Aldrich), thioglycolic acid (≥99%, Sigma Aldrich), hydrochloric acid (37 wt.% in H_2O, 99.999% trace metals basis, Sigma Aldrich), urea (≥99.5%, Sigma Aldrich), tin(II) chloride dihydrate (≥99.995% trace metals basis, Sigma Aldrich), Acetone (≥99.5%, semiconductor grade, thermo scientific), 2-propanol (≥99.5%, semiconductor grade, thermo scientific), Hellmanex III (Hellma Analytics), potassium chloride (>99%, Sigma ALdrich), 2-methoxyethanol (99.8%, anhydrous, Sigma Aldrich), lead(II) iodide (99.999% trace metals basis, perovskite grade, Sigma Aldrich), formamidinium iodide (>99.99%, Greatcellsolar), methylammonium bromide (>99.99%, Greatcellsolar), lead(II) bromide (99.999%, trace metals basis, Sigma Aldrich), methylammonium chloride (>99.99%, Greatcellsolar), *N*,*N*-dimethylformamide (99.8%, anhydrous, Sigma Aldrich), dimethyl sulfoxide (≥99.9%, anhydrous, Sigma Aldrich), diethyl ether (≥99.7 %, anhydrous, contains 1ppm BHT as inhibitor, Sigma Aldrich), *n*-hexylammonium bromide (>99 %, Greatcellsolar), chloroform (≥99%, anhydrous, contains amylenes as stabilizers, Sigma Aldrich), bis(trifluoromethane)sulfonimide (≥95.0 %, Sigma Aldrich), hydrogen peroxide$_{(aq)}$ (≥30%, Sigma Aldrich), Spiro-MeOTAD (>99,8%, Luminescence Technology), chlorobenzene (99.8%, anhydrous, Sigma Aldrich), hexane (95%,

anhydrous, Sigma Aldrich), Gold (Kurt J Lesker). All chemicals were used as received without further purification.

Synthesis of Spiro-MeOTAD(TFSI)$_4$ and Spiro-MeOTAD(TFSI)$_x$

Caution: bis(trifluoromethane)sulfonimide (HTFSI) is a toxic super acid.

Synthesis as described elsewhere.[19] Briefly, Bis(trifluoromethane)sulfonimide (HTFSI, 2 g, 7 mmol) was solved in 2 mL H_2O and 2 mL (20 mmol) 30% H_2O_2. 10 mL of Spiro-MeOTAD in chlorobenzene (0.5 mg/mL, 0.4 µmol/mL) was added and a biphasic mixture was received. The mixture was stirred at room temperature for 36 h. 7 mL of the organic solution was taken, and 40 mL hexane was added and centrifuged at 7000 rpm for 5 min. The precipitated Spiro(TFSI)$_4$ was dried with a heat gun for 3 min in ambient air.

For the hole transporting layer, typically, 5-10% of Spiro-MeOTAD was oxidized by mixing the above-obtained Spiro-MeOTAD(TFSI)$_4$ with 1.75 mL of Spiro-MeOTAD in chlorobenzene (70 mg/mL, 57 µmol/mL) and filtering the solution through a 0.22 µm polytetrafluoroethylene syringe filter.

Synthesis of methylammonium lead tribromide (MAPbBr$_3$)

Under nitrogen atmosphere, MABr (methylammonium bromide, 1.5252 g, 13.62 mmol) 10 mL *N*,*N*-dimethyl formamide were combined at room temperature. Pb(II)Br$_2$ (5 g, 13.62 mmol) was added. As the salts were dissolved completely, the solution was filtered (0.22 µm polytetrafluoroethylene syringe filter) and heated to 90 °C (stirring at 300 rpm). Crystals appeared in the first few minutes. The solution was stirred for about one hour. The crystals were gained by filtration, washed three times with diethyl ether, and transferred into a nitrogen glovebox.

Device fabrication

Substrate cleaning: In a Hellendahl staining vessel, 1 mL Hellmanex III and 49 mL deionized water were mixed, and substrates were submerged in the liquid. The substrates were ultrasonicated for 10 min at room temperature, following an ultrasonication sequence of solvents (deionized water, deionized water, acetone, 2-propanol) for 10 min each at 50 °C. The substrates were dried with a nitrogen gas gun.

SnO_2 deposition by chemical bath deposition:

Sodium Stannate trihydrate based: Substrates were placed in a Hellendahl staining vessel with 45 mL deionized water and tempered at the respective temperatures (55 °C, 65 °C, 75 °C, or 85 °C) for 20 min. A respective amount (16 mg, 160 mg, 1600 mg, or 3200 mg) of $Na_2SnO_3 \cdot 3\ H_2O$ was dissolved in 5 mL deionized water and added to the tempered vessel. The 3200mg $Na_2SnO_3 \cdot 3\ H_2O$ were dissolved in 10mL deionized water and added to 40mL deionized water in the tempered vessel. Substrates were removed once the solutions turned murky or the desired reaction time was reached. The substrates were cleaned by ultrasonication with a sequence of solvents (deionized water, deionized water, acetone, 2-propanol) for 10 minutes each at 50 °C. The substrates were dried with a nitrogen gas gun.

A typical synthesis uses 1600 mg (6 mmol) $Na_2SnO_3 \cdot 3\ H_2O$ dissolved in 5 mL deionized water and added to 45 mL deionized, tempered water at 85 °C. The reaction is stopped after 6 minutes by removing the substrates from the growth solution.

Tin(II) chloride based: In a Hellendahl staining vessel, urea (625 mg, 10.4 mmol), $Sn(II)Cl_2 \cdot 2H_2O$ (138 mg, 0.6 mmol), thioglycolic acid (12.5 µL, 0.1 mmol), hydrochloric acid (37 %; 625 µL, 7.5 mmol) and 50 mL deionized water are mixed. Substrates were placed in the vessel, which was kept

at 65 °C for about 12-14 h. The reaction was complete once the solution turned murky. The substrates were cleaned by ultrasonication with a sequence of solvents (deionized water, deionized water, acetone, 2-propanol) for 10 minutes each at 50 °C. The substrates were dried with a nitrogen gas gun.

MoO_x chemical bath deposition: 1 g (4.1 mmol) $Na_2MoO_4 \cdot 2\ H_2O$ was dissolved in 5 mL deionized water and added to 45 mL deionized, tempered water at a temperature of 85 °C in a Hellendahl staining vessel with FTO-coated substrates immersed in the solution. The reaction is stopped after 20 or 150 minutes by removing the substrates from the growth solution. The substrates were cleaned by ultrasonication with a sequence of solvents (deionized water, deionized water, acetone, 2-propanol) for 10 minutes each at 50 °C. The substrates were dried with a nitrogen gas gun.

SiO_2 chemical bath deposition: 1 g (8.2 mmol) Na_2SiO_3 was dissolved in 5 mL deionized water and added to 45 mL deionized, tempered water at a temperature of 85 °C in a Hellendahl staining vessel with FTO-coated substrates immersed in the solution. The reaction is stopped after 20 or 150 minutes by removing the substrates from the growth solution. The substrates were cleaned by ultrasonication with a sequence of solvents (deionized water, deionized water, acetone, 2-propanol) for 10 minutes each at 50 °C. The substrates were dried with a nitrogen gas gun.

Potassium chloride deposition: For some experiments, some substrates were annealed in an ambient atmosphere for one hour at 170 °C. Other substrates were not annealed. All samples were treated with oxygen plasma cleaning for 10 min. Subsequently, an aqueous KCl solution (0.745 mg/mL, 10 mM) was applied by spin-coating (acceleration: 3000 rpm, 3000 rpm, 30 s) onto the SnO_2 layer. Afterwards, the substrates were tempered for 10 min at 100 °C.

Perovskite deposition: Pb(II) iodide (704 mg, 1.53 mmol), formamidinium iodide (240 mg, 1.40 mmol), $MAPbBr_3$ (7 mg, 15 µmol), and methylammonium chloride (23 mg, 0.34 mmol) were dissolved in *N*,*N*-dimethylformamide (890 µL) and dimethylsulfoxide (110 µL). After filtration (0.22 µm polytetrafluoroethylene syringe filter), 70 µL of the solution was spin-coated (program: 1. 500 rpm, 5 s; 2. 1000 rpm, 14 s; 3. 5000 rpm, 30 s) on the substrates in a dry air atmosphere. 600 µL diethyl ether was added dynamically 10 s into the third spinning step. The substrates were annealed for one hour at 100 °C and 5 min at 150 °C. Once the substrates were at room temperature, *n*-hexylammonium bromide dissolved in chloroform (250 µL, 2.7 mg/mL, 15 mM) was spin-coated on top of the perovskite. After this 2D-perovskite surface treatment, the substrates were annealed for 10 min at 100 °C.

Finally, a small device-inactive area at the edge of the substrate was cleaned with 2-methoxyethanol-soaked cleanroom swabs to remove the hole transporting and perovskite layer for access to the FTO electrode.

Gold deposition: About 100 nm of gold was thermally evaporated from an alumina-coated molybdenum boat at a pressure below 5×10^{-6} mbar and a deposition rate of 0.5 Å/s for the first 10 nm and 1 Å/s for the remaining 90 nm.

Scanning electron microscopy

Electron microscopy images were recorded with a Zeiss Merlin Gemini 450.

Focused ion beam, transmission electron microscopy, and electron energy loss spectroscopy

The cross-section lamella for transmission electron microscopy was prepared with a FEI Helios NanoLab 600 FIB/SEM system.

The lamella was analyzed using a Thermo Fisher Themis Z G3 Cs-corrected S/TEM operated at 200 kV and equipped with a continuum EEL spectrometer. A 19 mrad convergence angle and 150 pA beam current were used (50 pA for images).

Powder x-ray diffraction

Diffraction patterns were obtained using a PANalytical X'Pert Pro powder X-ray diffractometer, operating with a 1.8 kW Cu–Kα X-ray source and aligned in Bragg-Brentano geometry.

Current-Voltage measurement

The solar cells were protected by applying a polyimide tape with silicone adhesive (7639A12, McMaster-Carr) over the backside of the substrate and gold electrodes. The cells were placed in the measurement setup under ambient air, where the current was measured with a 2420 source measurement unit (Keithley) by applying a voltage. An Oriel Sol3A solar simulator (Newport) combined with a Xenon arc lamp was used for illumination. As a reference, an Oriel reference silicon solar cell (Newport) was measured to calibrate the irradiance to 1 sun (AM1.5). To stabilize the temperature of the solar cell, a ThermoStation P500 Peltier cooler (McScience) kept the temperature at 20 °C.

References

1 NREL - Best Research-Cell Efficiency Chart, https://www.nrel.gov/pv/assets/pdfs/best-research-cell-efficiencies.pdf, (accessed 28 June 2024).

2 J. J. Yoo, G. Seo, M. R. Chua, T. G. Park, Y. Lu, F. Rotermund, Y. K. Kim, C. S. Moon, N. J. Jeon, J. P. Correa-Baena, V. Bulović, S. S. Shin, M. G. Bawendi and J. Seo, *Nature 2021 590:7847*, 2021, **590**, 587–593.

3 A. Uddin and H. Yi, *Solar RRL*, 2022, **6**, 2100983.

4 L. Zhang, H. Bin Wu and X. Wen Lou, *Mater Horiz*, 2013, **1**, 133–138.

5 E. H. Anaraki, A. Kermanpur, L. Steier, K. Domanski, T. Matsui, W. Tress, M. Saliba, A. Abate, M. Gräzel, A. Hagfeldt and J.-P. Correa-Baena, *Energy Environ Sci*, 2016, **9**, 3128–3134.

6 T. Bu, X. Liu, Y. Zhou, J. Yi, X. Huang, L. Luo, J. Xiao, Z. Ku, Y. Peng, F. Huang, Y.-B. Cheng and J. Zhong, *Energy Environ. Sci*, 2017, **10**, 2509.

7 Y. Lu, C. Shih, S. Tan, M. J. Grotevent, L. Wang, H. Zhu, R. Zhang, J.-H. Lee, J.-W. Lee, V. Bulović and M. G. Bawendi, *Advanced Materials*, 2023, **35**, 2304168.

8 N. Ren, L. Tan, M. Li, J. Zhou, Y. Ye, B. Jiao, L. Ding and C. Yi, *iEnergy*, 2024, **3**, 39–45.

9 T. Schneller, R. Waser, M. Kosec and D. Payne, *Chemical solution deposition of functional oxide thin films*, Springer-Verlag Wien, 2013.

10 Y. Yang, Y. Wang and S. Yin, *Appl Surf Sci*, 2017, **420**, 399–406.

11 S. Anuchai, S. Phanichphant, D. Tantraviwat, P. Pluengphon, T. Bovornratanaraks and B. Inceesungvorn, *J Colloid Interface Sci*, 2018, **512**, 105–114.

12 H. Uchiyama, H. Ohgi and H. Imai, *Cryst Growth Des*, 2006, **6**, 2186–2190.

13 S. Supothina, M. R. De Guire, T. P. Niesen, J. Bill, F. Aldinger and A. H. Heuer, *MRS Online Proceedings Library*, 1999, **576**, 203–208.

14 G. Oldfield, T. Ung and P. Mulvaney, *Advanced Materials*, 2000, **12**, 1519–1522.

15 R. Medhi, C. H. Li, S. H. Lee, M. D. Marquez, A. J. Jacobson, T. C. Lee and T. R. Lee, *ACS Appl Nano Mater*, 2019, **2**, 6554–6564.

16 P. Holzhey, M. Prettl, S. Collavini, C. Mortan and M. Saliba, *Scientific report*, 2023, **13**, 6375.

17 N. Li, K. Du, G. Liu, Y. Xie, G. Zhou, J. Zhu, F. Li and H. M. Cheng, *J Mater Chem A Mater*, 2013, **1**, 1536–1539.

18 M. S. Moreno, R. F. Egerton and P. A. Midgley, *Phys Rev B*, 2004, **69**, 233304.

19 M. J. Grotevent, Y. Lu, T. Šverko, M. C. Shih, S. Tan, H. Zhu, T. Dang, J. K. Mwaura, R. Swartwout, F. Beiglböck, L. Kothe, V. Bulović and M. G. Bawendi, *Adv Energy Mater*, 2024, 2400456.

Conflict of Interest

The authors declare no conflict of interest.

Data availability

The data supporting this article have been included as part of the ESI.

Author Contributions

M.J.G. and M.G.B. conceived the project. L.K. fabricated the tin oxide films with scientific contributions of M.T. M.J.G. fabricated solar cells from the SnO_2 coated substrates and performed electrical characterization of the devices. Y.L. recorded the scanning electron microscopy images. C.K. performed the X-ray diffraction measurements. M.-C.S. and S.T. contributed to the critical scientific discussions about the perovskite composition and decomposition pathways. M.J.G. and L.K. wrote the manuscript with contributions from all authors. All authors have discussed the results and approved the final version of the manuscript.

Acknowledgments

We thank First Solar for financial support and fruitful discussions. This work was performed in part at the MIT nano Characterization Facilities. We thank Dr. Zhenyuan Zhang at MIT.nano for

fabricating the transport layer cross-section and Dr. Aubrey Penn at MIT.nano for the transmission electron microscopy study, including electron energy loss spectroscopy.

M.J.G. acknowledges the support of the Swiss National Science Foundation through the Early Postdoc.Mobility Fellowship grant #P2EZP2_199844. L.K. acknowledges the support of the Fulbright Germany Foundation through the D-Visiting Student Researchers (Doktorand:innen) grant and Woehler Technik GmbH for sponsoring. Y.L. and M.-C.S. acknowledge the support by the U.S. Department of Energy, Solar Energy Technologies Office award no. DE-EE0009512.